JOURNAL OF MATERIALS SCIENCE 27 (1992) 2345–2352

Morphology and crystallinity changes during PPS doping

R. E. S. BRETAS, M. C. B. DE JESUS, G. J. LUNARDI
Department of Materials Engineering, Universidade Federal de São Carlos, Rod Washington Luiz, 13560 São Carlos, São Paulo, Brazil

Poly(*p*-phenylene sulphide), PPS, was gas- and solution-doped with $AlCl_3$ and I_2. Morphology and crystallinity changes introduced by the dopant were analysed. The solvent has an important role in the preservation of the original morphology and in the final electrical conductivity achieved. The doping increased the crystallinity index, and it is believed that both dopants were intercalated between the lamellae, decreasing the interplanar spacing, but not destroying the intracrystalline order. The highest conductivity was achieved with the system LDC–$AlCl_3$–CH_3NO_2.

1. Introduction

Poly(*p*-phenylene sulphide), PPS, is a polymer that can be rendered conductive after chemical doping with AsF_5, SO_3 or TaF_5. This doping probably allows the dopant ion to intercalate between the macromolecules, followed by an oxi-reduction reaction which produces polarons and bipolarons (depending on the dopant concentration).

The PPS unit cell is orthorhombic: the phenyl groups are located at $\pm 45°$ relative to the C–S–C plane (1 0 0 plane). This non-planar configuration, allied to an energy band gap of 6.3 eV, makes ionization difficult; it is usually necessary to employ strong chemical dopant agents, toxics and corrosives, to achieve high levels of conductivity. It is believed that the interaction of the phenyl π orbitals with the sulphur p orbitals is important for providing the delocalized electronic system necessary for high conductivities in the doped state.

There are some proposed mechanisms of conduction in PPS. Baughman *et al.* [1] proposed that, at low doping levels, the formation of charge transfer complexes occurs, and at high doping levels there is also the formation of dibenzothiophene linkages (intrachain bridging) predominating over interchain cross-linking. Clarke *et al.* [2] suggested the possibility of intermolecular cross-linking between phenyl rings, forming poly-*p*-phenylene structures across the polymer chains. Friend and Giles [3] predicted the initial formation of polaron states along the polymer chain, at low doping levels, followed by the loss of these states on increased doping when pairs of polarons coalesce to form bipolarons. Tsukawato and Matsumara [4] suggested an electron transfer from the sulphur atom upon doping. This charge transfer brings about an increase in the interaction between sulphur atoms and phenyl rings, and increases the double-bond character of the C–S bond. Thus, the conjugated system is formed via the sulphur atoms in the PPS chain. Later, Tsukamoto *et al.* [5] showed that the C–S–C angle gets wider (125°) upon doping, enhancing the overlapping between the sulphur and the phenyl ring orbitals.

The influence the morphology and crystallinity have on PPS doping has been less studied. Kawano *et al.* [6] showed that the dopants TCNE and I_2 exist mainly in the amorphous region and that electronic conduction takes place in TCNE-doped PPS but ionic conduction in I_2-doped PPS. Tsukamoto and Matsumara [7] suggested that doping proceeds also in the amorphous region of PPS and that the lower the crystallinity of starting PPS, the easier is the doping.

In this work morphology and crystallinity changes, after gas- and solution-doping were studied, in order to clarify the influence these two parameters and the solvent have on the final conductivity achieved after doping.

2. Experimental procedure

2.1. Sample preparation

The PPS (Ryton V1, Philips Petroleum) was distilled by Soxhlet distillation using tetrahydrofuran (48 h).

Films with different morphologies and degrees of crystallinity were obtained by the following procedures:

(i) Solvent casting (CS): films were produced by solvent evaporation from a PPS–diphenyl ether solution ($c = 30\ g\,l^{-1}$, $T = 230\,°C$).

(ii) Low degree of crystallinity (LDC): after melting ($T = 295\,°C$), the film was quenched to $-12\,°C$.

(iii) Non-isothermally crystallized (MDC and HDC): after melting, the film was cooled to room temperature at different rates (MDC, $3\,°C\,min^{-1}$; HDC, $0.7\,°C\,min^{-1}$).

(iv) Isothermally crystallized from the glassy state (CI): films were obtained by isothermal crystallization of the LDC samples in a silicone oil bath at 230 °C.

(v) Isothermally crystallized from the melt (CIM):

0022–2461

after melting the film was maintained at 250 °C for 8 h, under vacuum, and cooled as for the MDC samples. The film thickness was 30–45 μm, measured by an Elcometer Thickness Gauge 150.

2.2. Characterization

Due to the insolubility of PPS at room temperature, its molecular weight was indirectly measured using its melt flow Index [8]: we obtained $M_w = 25\,300$, $M_n = 11\,000$ (Philips Petroleum), M.W.D. = 2.3.

Polarized-light optical, PLO (Nikon) and scanning electron micrographs (Cambridge Stereoscan S4-10) of the films were obtained before and after the doping.

Crystallinity indices, T_g and T_m, were obtained by differential scanning calorimetry, DSC (Dupont TA 990, 10 °C min^{-1}), density gradient (ASTM D1505, $\rho_c = 1.439$ g cm^{-3}, $\rho_a = 1.308$ g cm^{-3} [9] and wide-angle X-ray scattering, WAXS (Philips PW 1130/00, CuK_α, Ni filter). Chemical modifications introduced by the doping were analysed by infrared spectroscopy (Perkin–Elmer 1750 FTIR).

2.3. Doping and conductivity measurements

Gaseous doping was performed with $AlCl_3$–HCl at room temperature, following the Sholtes procedure [10].

For solution doping, three different solutions were used: $AlCl_3$–CH_2Cl_2 (0.85 M), $AlCl_3$–CH_3NO_2 (1 M) and I_2–CCl_4 (0.26 g l^{-1}), at 30 °C under gaseous N_2.

The conductivity was measured using a van der Pauw arrangement [11]. The four Au metallized electrodes were attached to Au strands with Electrodag 417SS (Acheson, Brazil) and connected to a 30 V voltage stabilizing source (Labo FR2515), a high-resistivity meter (HP 4329A) and an electrometer (Keithley 610-C).

3. Results and discussion

3.1. Optical polarized light and scanning electron microscopy

Fig. 1 shows PLO micrographs of four samples, before doping. Fig. 2 shows SEM micrographs of the same samples, before doping. Holes on the CS surface produced by solvent evaporation can be observed. The MDC and HDC morphologies are both globular.

Fig. 3 shows the initial (after 2 min) and final (after 10 min) $AlCl_3$–CH_2Cl_2 doping stages of a CIM sample. In Fig. 3b and c it can be observed that the dopant agent penetrates first into the interspherulitic and interlamellar region within the spherulites. This rapid diffusion is probably due to a high degree of intracrystallite disorder. Fig. 3d shows the complete destruction of the crystalline morphology. The

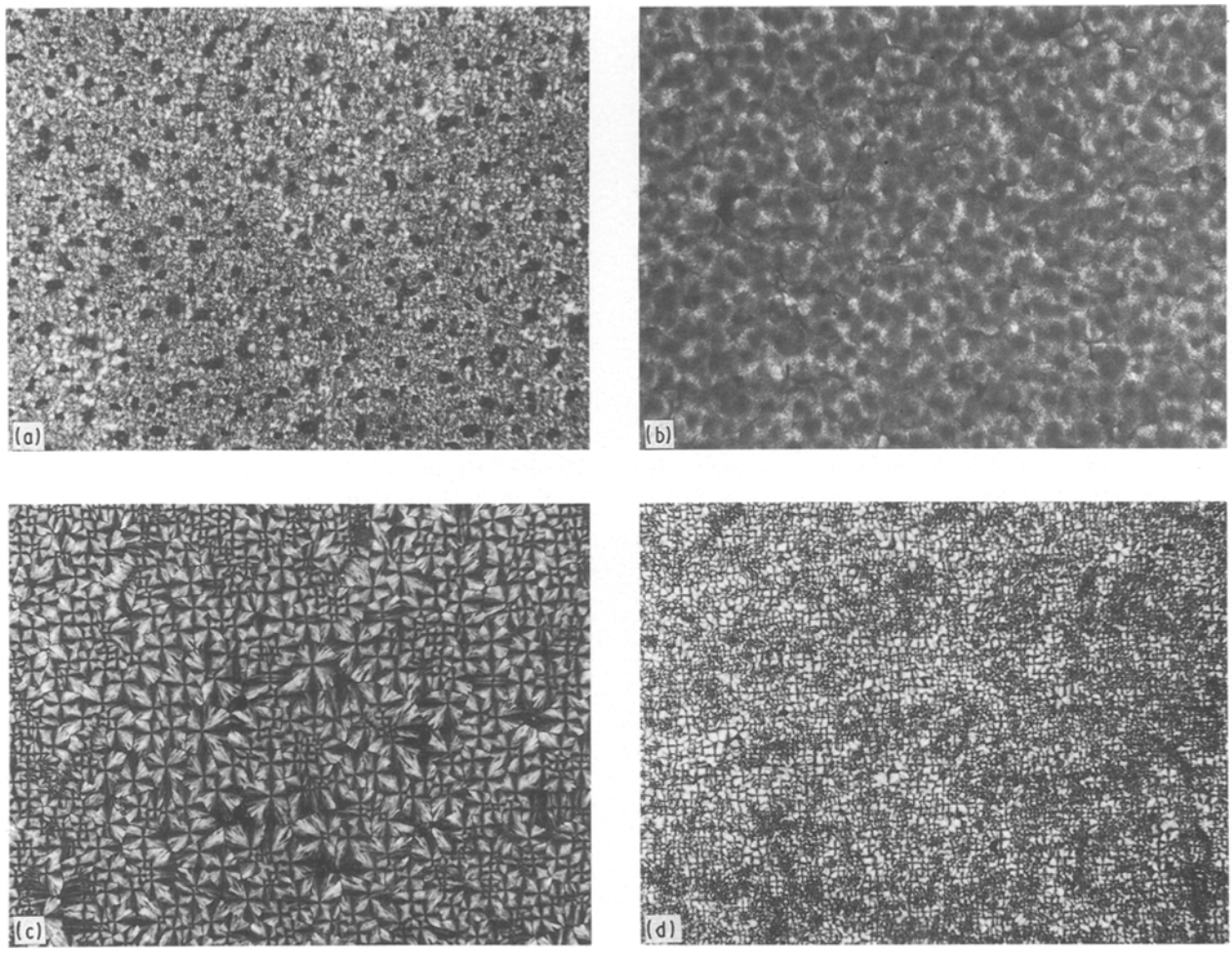

Figure 1 Polarized light micrographs: (a) CS, (b) HDC, (c) CI230, (d) MDC (all 240 ×).

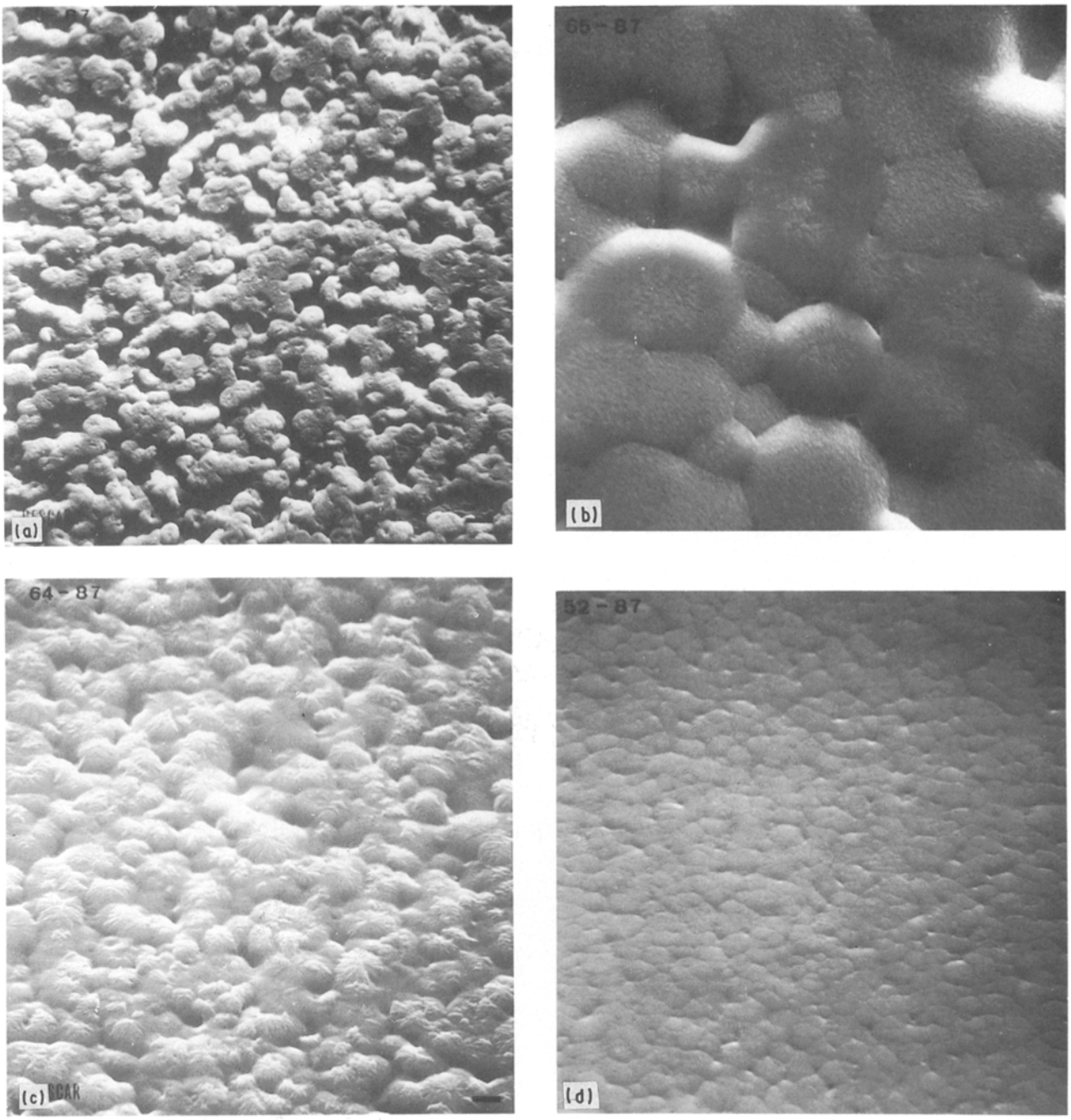

Figure 2 Scanning electron micrographs: (a) CS (440 ×), (b) HDC (4500 ×), (c) CI230 (4500 ×), (d) MDC (400 ×).

$AlCl_3$–CH_2Cl_2 attack on PPS is not due solely to the $AlCl_3$, but also to the swelling action of CH_2Cl_2.

Fig. 4 shows SEM micrographs of the MDC samples after doping. The $AlCl_3$–HCl doping produced microporosity, but did not destroy the morphology; $AlCl_3$–CH_3NO_2 promoted solvent stress cracking, but also did not destroy the sample; finally, I_2–CCl_4 only swelled the spherulites.

3.2. Crystallinity data

3.2.1. WAXS data

Fig. 5 shows the normalized WAXS (without air scattering and background) of some of the samples. The higher-crystallinity samples have two main peaks at $2\theta = 21.2$ and 19.5°. Using Brady's method [12] the crystallinity index C_i was measured between 17 and 23° by using the ratio of the areas under the diffraction peaks:

$$C_i = \frac{A_{\text{crystalline}}}{A_{\text{crystalline}} + A_{\text{amorphous}}} \times 100$$

In this range the $AlCl_3$ (powder) has some diffraction peaks, as shown in Table I. None of these peaks could be separated from the PPS data; however, the major contributions to the PPS crystallinity index are given by the two main peaks at 21–22° and 19–20°, as shown in Fig. 5. We assume that the $AlCl_3$ is in an ionic form (probably $AlCl_4^-$ [10]) in the polymer. If some pure $AlCl_3$ is present, its contribution to the crystallinity index is going to be almost null, because in the above-mentioned ranges $AlCl_3$ does not present any intensity

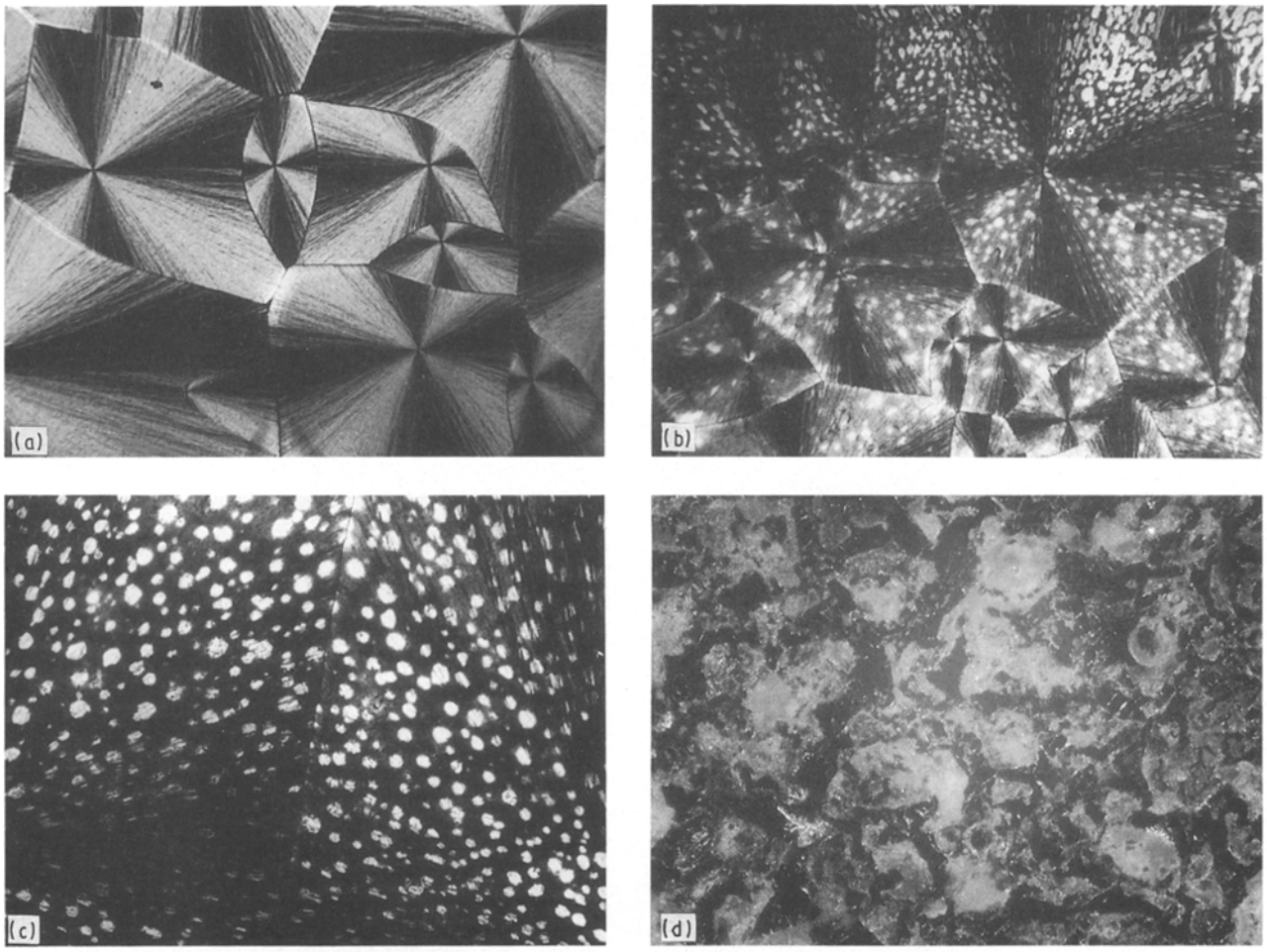

Figure 3 Polarized light micrographs of $AlCl_3$–CH_2Cl_2 doping of, CIM: (a) before doping (240 ×), (b) after 2 min (240 ×), (c) interspherulitic region (800 ×), (d) after 10 min (240 ×).

peak. The calculated crystallinity indices are shown in Table II.

Fig. 6 shows the normalized WAXS of LDC samples after doping. Both dopings turn the samples more crystalline, as can be seen by the gradual growth of "peaks" around $2\theta = 22$ and 19°. It seems that both dopants plasticize the PPS amorphous region, lowering the T_g and inducing the nucleation and recrystallization of PPS, even at 30 °C. The doping decreases the interplanar spacing, indicating a small lateral compression of the lattice due to dopant intercalation. However, the lattice order was not disrupted, and we believe that these dopants will remain in the amorphous region, even at high doping levels. This same behaviour can be observed with the MDC and HDC samples, as shown in Figs 7 and 8. Iodine decreases the interplanar spacing more strongly than $AlCl_3$.

Fig. 9 shows a PLO micrograph of an LDC sample after I_2 doping. A birefringence increase at some points can be noted.

The degree of cross-linking will increase with the crystallinity index, because PPS cures in the presence of air at 295 °C [13]. This cure will limit dopant penetration and intercalation. This is probably the reason for the low increase of crystallinity induced by the dopant in the MDC and HDC samples.

3.2.2. DSC and density gradient column data

Table III presents crystallinity data from DSC and density gradient measurements before and after doping. The doping with $AlCl_3$–CH_2Cl_2 and $AlCl_3$–HCl degraded the samples. They turned into a black green powder and thermal property measurements after the doping were unsuccessful.

The DSC curves after I_2 doping showed a broad exothermic peak around $T = 135$ °C, probably due to I_2 melting, as seen in Fig. 10. It can be seen that the presence of I_2 inhibits cold crystallization (around $T = 128$ °C), probably because it induces the formation of a higher amount of cross-linking in the "rigid amorphous region" [14] during the temperature scanning. The DSC data have to be analysed very carefully: it is necessary to recall that PPS can be oxidatively and thermally cured [13], and there is evidence that the dopant itself can also induce cross-linking [1]. Thus, the samples were oxidatively cured during their preparation and thermally cured during the calorimetry test. These treatments certainly changed their initial crystallinity values.

3.3. Infrared spectroscopy

Some aspects of the infrared absorption band data should be evidenced:

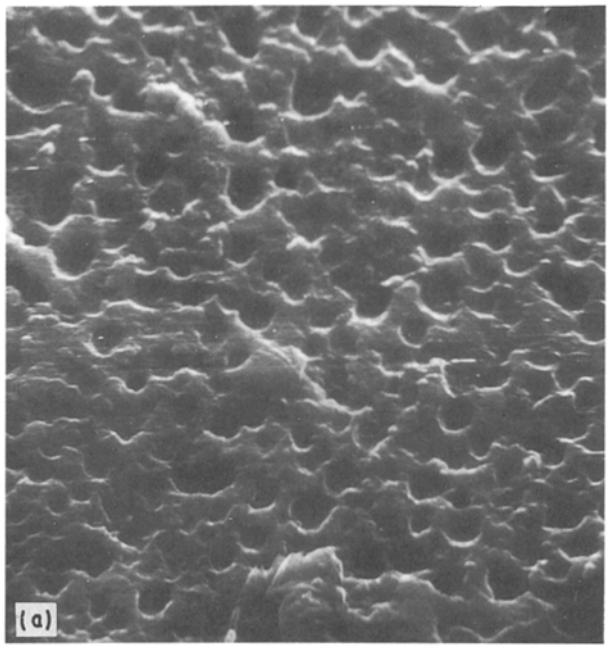

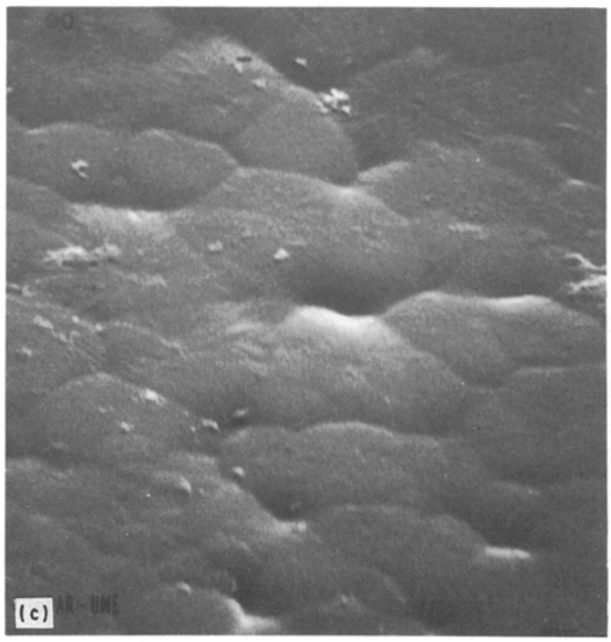

Figure 4 Scanning electron micrographs of MDC samples: (a) after $AlCl_3$–HCl doping (1800×), (b) after $AlCl_3$–CH_3NO_2 doping (1900×), (c) after I_2–CCl_4 doping (1800×).

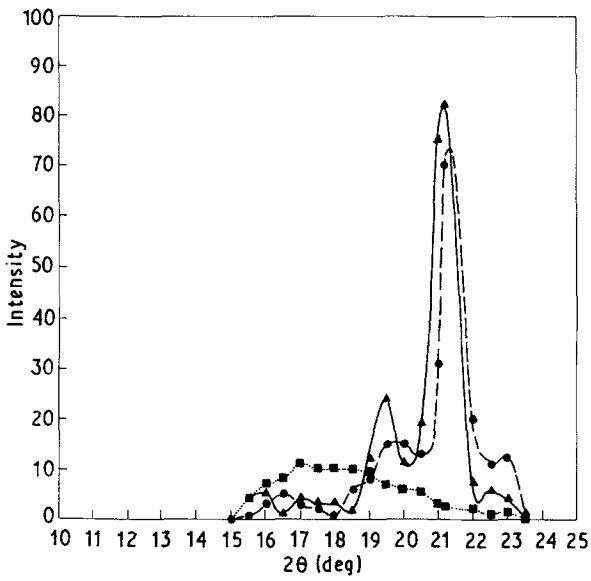

Figure 5 Normalized WAXS of some PPS samples: (▲) HDC, (■) LDC, (●) MDC.

1. The doping introduces a new, small band at 3010 cm^{-1}, near the 3065 cm^{-1} band (CH aromatic, stretch); another small band at 1350 cm^{-1}, and one at 1260 cm^{-1}. This last one is characteristic of = C–O–C– (C aromatic), indicating PPS cure [7]. The increasing absorption at 1230 cm^{-1} can be a sign of 1, 2, 4 trisubstitution.

2. The 820 cm^{-1} band (benzene 1, 4 disubstituted) becomes larger and broader (830–740, 810–830 and 810–830) upon I_2 doping, indicating an increase in benzene trisubstitution.

3.4. Conductivity data

Table IV shows the maximum conductivity obtained after doping. The maximum conductivity does not seem to be affected by the degree of crystallinity when the dopant is $AlCl_3$–HCl (gaseous). The doping with $AlCl_3$–CH_2Cl_2, $AlCl_3$–CH_3NO_2 or I_2 was affected by the amount of crystallinity, the conductivity being higher when the sample had an initially low crystallinity content.

The conductivity will depend on the number and mobility of the charge carriers, polarons or bipolarons. After the doping with I_2 and $AlCl_3$–CH_3NO_2, the samples had a weight increase as shown in Table V.

The LDC sample has more supramolecular defects (cilia, entanglements, irregular chain folding) than the MDC and HDC samples. These defects can eventually

TABLE I $AlCl_3$ WAXS data

I/I_0 (%)	2θ (deg)
100	15.11
12	17.3
20	17.99
12	20.13
6	23.04

TABLE II Samples Crystallinity Indices (C_i) from WAXS

Sample	C_i (%)
LDC	0
MDC	76.1
HDC	79.8
LDC–$AlCl_3$/2 h	63.8
LDC–$AlCl_3$/5 h	48.0
LDC–I_2	44.6
MDC–$AlCl_3$/2 h	77.7
MDC–$AlCl_3$/5 h	83.1
MDC–I_2	79.0
HDC–$AlCl_3$/2 h	77.5
HDC–$AlCl_3$/5 h	78.5
HDC–I_2	83.5

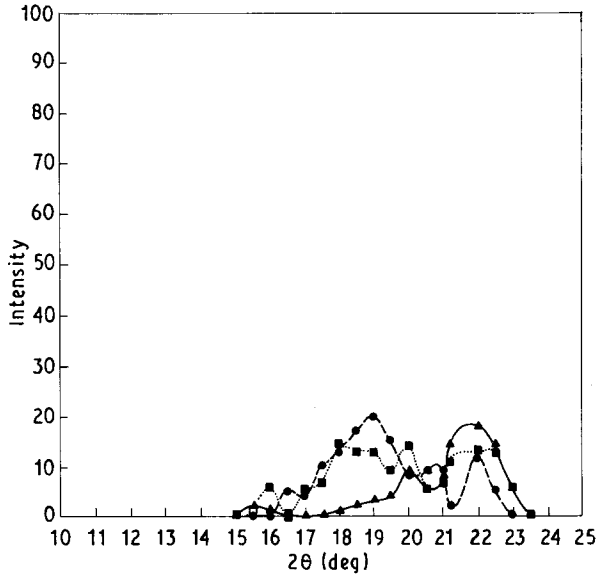

Figure 6 Normalized WAXS of LDC samples after doping: (▲) LDC–$AlCl_3$/2 h, (■) LDC–$AlCl_3$/5 h, (●) LDC–I_2.

trap the charge carrier and reduce its mobility. However, this sample, in turn, will have a higher number of these carriers, because its amount is proportional to the dopant concentration. The result is a conductivity higher than the high-crystallinity samples.

Figs 11 and 12 show the conductivity versus doping time of some PPS samples during $AlCl_3$–CH_3NO_2 and I_2–CCl_4 doping. A maximum can be observed in the MDC and HDC $AlCl_3$ doping curves, after 2 h of doping. It is believed that continuous dopant penetration introduces more defects into the lamellae, like dislocations in a macromolecular row, that will trap the charge carriers, decreasing the conductivity. That

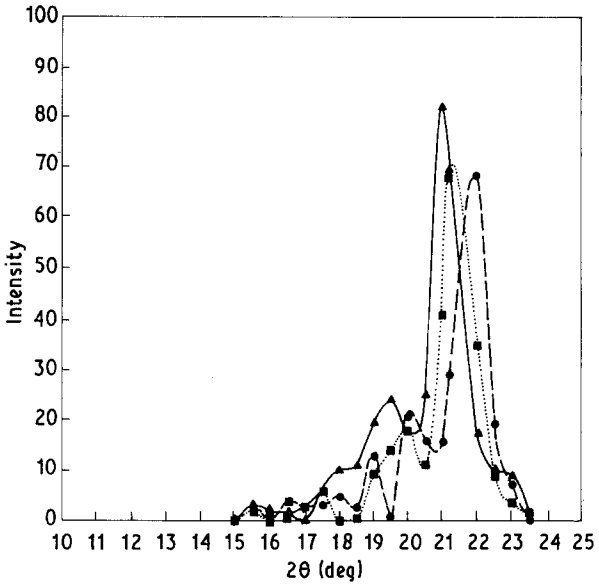

Figure 7 Normalized WAXS of MDC samples after doping: (▲) MDC–$AlCl_3$/2 h, (■) MDC–$AlCl_3$/5 h, (●) MDC–I_2.

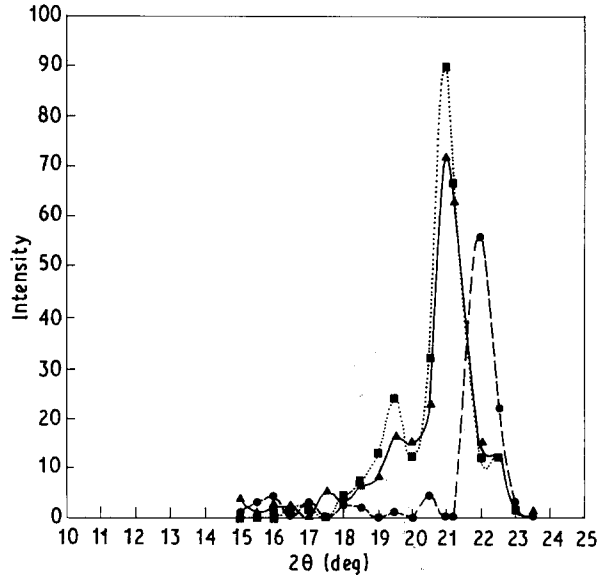

Figure 8 Normalized WAXS of HDC samples after doping: (▲) HDC-$AlCl_3$/2 h, (■) HDC–$AlCl_3$/5 h, (●) HDC–I_2.

TABLE III Degree of crystallinity, w

Sample	Before doping			After doping	
	w^a (%)	w^b (%)	T_g (C°)	w (%)[c] $AlCl_3$–CH_3NO_2	w (%)[d] I_2
Powder	–	62.2	–	–	–
CS	61	–	–	–	–
CIM	62	–	–	–	–
LDC	13	24.9	84	22.6/35	37
MDC	51	48.8	119[e]	37.1/50.81	63.2
HDC	–	81.2	127[e]	52.9/43.2	67.1
CI	46	–	–	–	–

[a] By density gradient.
[b] By DSC; ΔH (PPS, 100% crystalline) = 80 J g^{-1}.
[c] By DSC, after 2 and 5 h, respectively.
[d] By DSC, after 300 h.
[e] By dynamic mechanical thermal analyser (Polymers Laboratory).

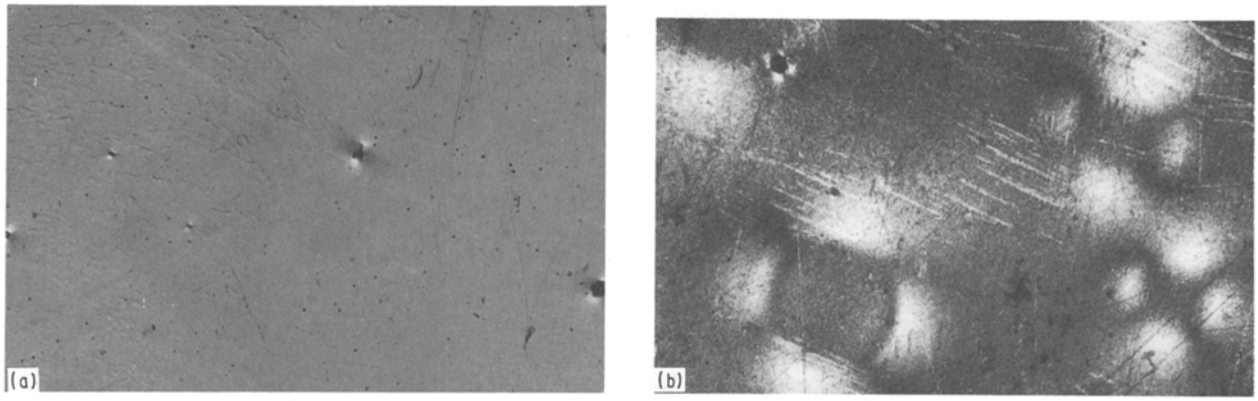

Figure 9 LDC samples (a) before and (b) after I_2 doping.

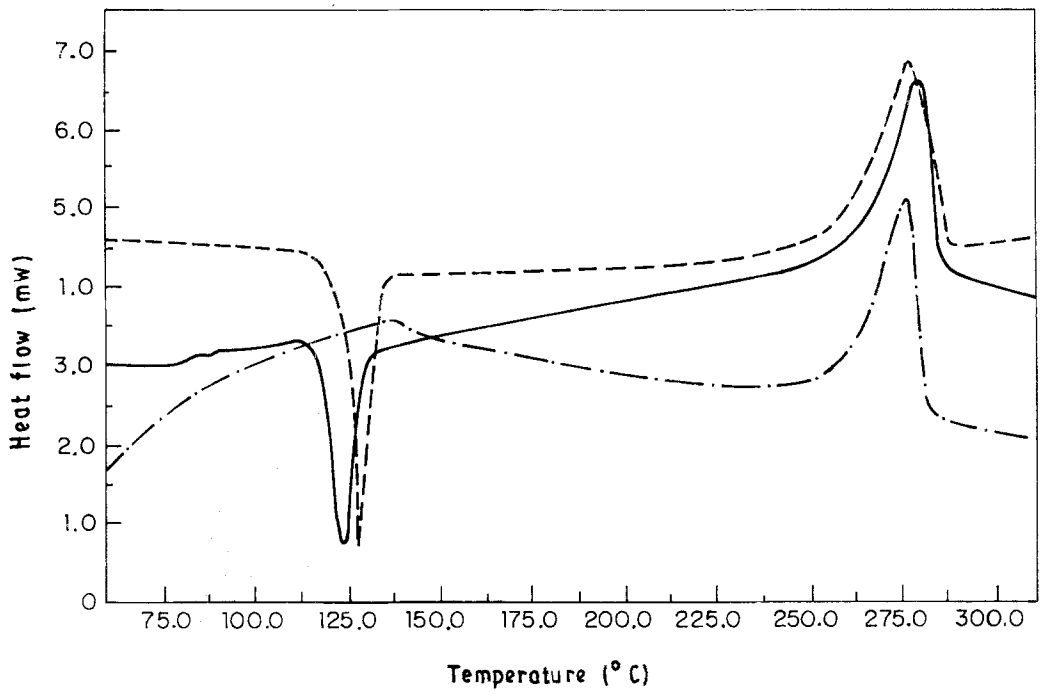

Figure 10 DSC of LDC samples: (– – –) before doping, (——) LDC–$AlCl_3$, (– · –) LDC–I_2.

TABLE IV Maximum conductivity after doping

Sample	$AlCl_3$–HCl	$AlCl_3$–CH_2Cl_2[a]	$AlCl_2$–CH_2NO_2[b]	I_2[c]
CS	3.4×10^{-4}	1.7×10^{-8}	–	–
CIM	0.8×10^{-4}	3.4×10^{-8}	–	–
LDC	6.5×10^{-4}	7.2×10^{-6}	2.4×10^{-1}	9.0×10^{-6}
MDC	2.4×10^{-4}	2.1×10^{-8}	1.8×10^{-4}	8.2×10^{-7}
HDC	–	–	1.3×10^{-4}	9.2×10^{-9}
CI	5.1×10^{-4}	1.9×10^{-8}	–	–

[a] Point when the polymer began to degrade.
[b] After 300 min.
[c] After 300 h.

TABLE V Weight increase of the samples after doping

Sample	Weight increase (%) I_2	Weight increase (%) $AlCl_3$–CH_3NO_2
LDC	47.03	6.83
MDC	1.03	3.67
HDC	0.97	3.20

is the reason why the crystallinity index remains almost unaffected after the doping of these samples.

4. Conclusions

The characterization of doped samples will need further analysis. However, some points can be evidenced:

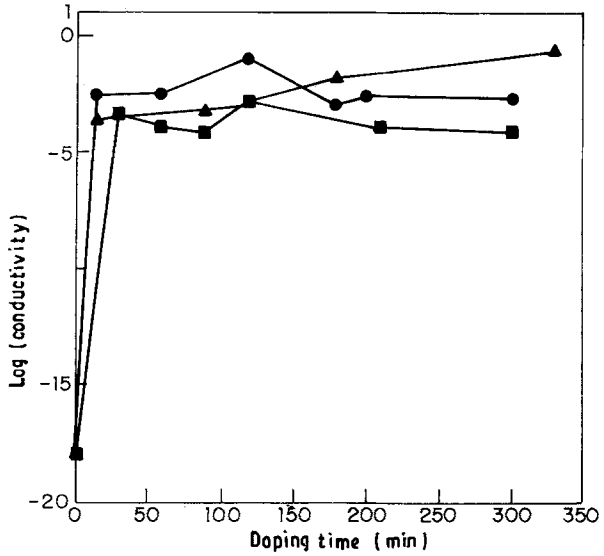

Figure 11 Conductivity versus $AlCl_3$–CH_3NO_2 doping time: (▲) LDC, (■) MDC, (●) HDC.

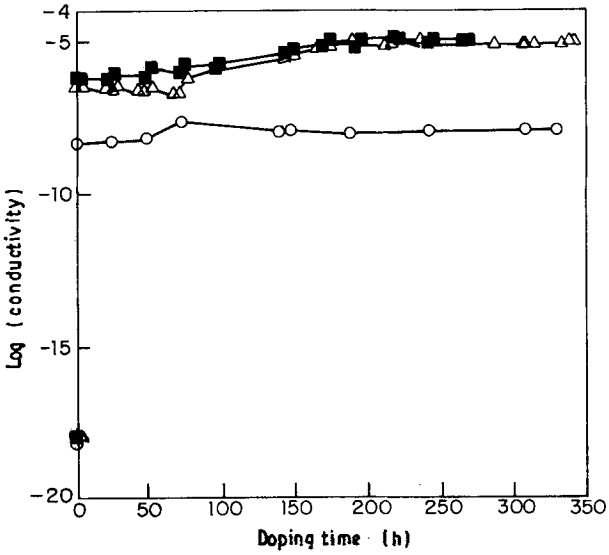

Figure 12 Conductivity versus I_2 doping time: (■) LDC, (△) MDC, (○) HDC.

1. The $AlCl_3$–CH_2Cl_2 doping system was the only one that did not preserve the original morphology, showing that the solvent has a fundamental role. CH_2Cl_2 was the only solvent that, without the dopant, swelled the PPS [15]. Its action allowed the dopant to penetrate into the interspherulitic and interlamellar region within the spherulites, destroying the crystalline morphology.

2. Both dopants, $AlCl_3$ and I_2, intercalated between the lamellae, decreasing the interplanar spacing. I_2 decreased this spacing more than $AlCl_3$. However, this intercalation did not destroy the intracrystalline order.

3. The PPS cure limited dopant penetration and intercalation.

4. The maximum conductivity is not affected by the initial crystallinity when the dopant is $AlCl_3$–HCl. However, when the dopant is $AlCl_3$–CH_2Cl_2, $AlCl_3$–CH_3NO_2 or I_2 a higher conductivity is achieved with the lower initial crystallinity sample.

5. The highest level of conductivity was achieved with the LDC–$AlCl_3$–CH_3NO_2 system, showing that the initial morphology and crystallinity influence the final conductivity. The doping increased the LDC crystallinity index, by reducing T_g and inducing nucleation and recrystallization. This shows that even in a structure with an originally high amount of defects, these initial defects do not play an important role. A more important factor is the easy penetration or sorption of the dopants (because of the higher amount of amorphous regions), and the subsequent ordering and even intra- and intermolecular cross-linking on these regions, that will allow the retention of the dopants during more time (allowing a lower desorption) and will increase intra- and intermolecular electron hopping.

Acknowledgements

The authors wish to express their gratitude to Pirelli S/A do Brasil, FAPESP and CAPES for their financial support.

References

1. R. H. BAUGHMAN, J. L. BRÉDAS, R. R. CHANCE, R. L. ELSENBAUMER and W. SHACKLETTE, *Chem. Rev.*, No. 82 (1982) 209.
2. T. C. CLARKE, K. K. KANAZAWA, V. Y. LEE, J. F. RABOLT, J. R. REYNOLDS and G. B. STREET, *J. Polym. Sci., Polym. Phys. Edn* **20** (1982) 117.
3. R. H. FRIEND and J. P. M. GILES, *J. Chem. Soc., Chem. Commun.* (1984) 1101.
4 J. TSUKAMOTO and K. MATSUMURA, *Jpn. J. Appl. Phys.* **24** (1985) 974.
5. J. TSUKAMOTO, S. FUKUDA, K. TANAKA and T. YAMABE, *Synth. Met.* No. 17 (1987) 673.
6. M. KAWANO, S. SHICHIJYO, T. HORIUCHI, K. MATSUSHIGE and T. TAKEMURA, *Jpn. J. Appl. Phys.* **23** (1984) 979.
7. J. TSUKAMOTO and K. MATSUMURA, *ibid.* **23** (1984) L584.
8. C. J. STACY, *J. Appl. Polym. Sci.* **32** (1986) 3959.
9. J. Z. CHEN and S. C. JIANG, *Acta Chim. Sinica* **38**(1) (1980) 50.
10. V. L. SHOLTES, PhD thesis, University of Pennsylvania (1983).
11. R. L. ELSENBAUMER and L. W. SHACKLETTE, In "Handbook of Conducting Polymers", Vol. 1, edited by J. A. Skolteim (Dekker, New York, 1986) pp. 213–265.
12. D. G. BRADY, *J. Appl. Polym. Sci.* **20** (1976) 2541.
13. R. T. HAWKINS, *Macromolecules* **9** (1976) 189.
14. S. Z. D. CHENG, Z. Q. WU and B. WUNDERLICH, *ibid.* **20** (1987) 2802.
15. R. E. S. BRETAS and G. LUNARDI, in Proceedings of 8th CBECIMAT, Campinas (1988) pp. 355–358.

Received 9 November 1990
and accepted 26 July 1991